A Novel Dynamic Friction Experiment Using a Modified Kolsky Bar Apparatus

by H. D. Espinosa, A. Patanella and M. Fischer

ABSTRACT—A novel dynamic friction experiment using the Kolsky bar concept was developed. The technique is complementary to the plate impact and other macroscopic friction experiments in the sense that sliding velocities and pressures not attainable otherwise can be investigated. The experimental results reported in this article show that the technique provides accurate and repeatable measurement of time-resolved friction. The apparatus is simpler and easier to operate than the plate impact facility. However, it cannot achieve the same level of contact pressure. Several material pairs have been investigated. In particular, the kinetic friction coefficient of Ti-6Al-4V sliding against WC/Co (cermet) and 4340 steel sliding against WC/Co were measured and compared with the values reported by Prakash and Clifton in 1993. Atomic force microscopy is used to characterize the surface topography before and after the friction tests.

KEY WORDS—Kolsky bar, dynamic friction, manufacturing, wear

Introduction

Contact and friction between surfaces occur in many engineering applications as well as in the response of materials with evolving microstructures, for example, comminution of brittle materials, fiber-matrix debonding in composite materials, delamination of coatings and crack propagation in bimaterial and multilayered materials. Despite the many excellent contributions in the area of friction and wear of materials,[1,2] unified models that can accurately predict the friction behavior of surfaces in contact are not available. Some of the difficulties in achieving such unified model are (1) the fact that tribology is a multiscale phenomenon affected by the surface geometrical structure, the surface forces and the properties of the surface material itself; (2) the interaction between these effects and surface chemistry; and (3) the lack of experiments capable to explore the time response of the friction event.

A wide variety of experiments are required to fully characterize the friction phenomena. In such experiments, it is necessary to simulate the local conditions of pressure, tangential and normal velocities, surface characteristics, chemistry and temperature present in the applications of interest. These conditions need to be realized in a simple geometry for which the local interface conditions can be easily measured. In this way, mathematical models of the frictional behavior of interfaces can be used to describe the phenomena. In turn, these models can be incorporated in computational simulations to gain insight into the main features associated with engineering applications in which contact and friction between bodies are relevant.

Several experimental techniques are available for the study of dynamic friction. It is important to differentiate between nano/micro-tribology and macro-tribology experiments. Nano/micro-tribology experiments include nano-scratching and adhesion force measurements with an atomic force microscope (AFM)[3] or a surface force apparatus.[4,5] In these tests, atomic and molecular interaction forces are measured from which the frictional response of lubricated and unlubricated surfaces can be investigated.[6]

The macro-tribology experiments are divided into the following groups:

- Pressure-shear plate impact friction experiments[7,8] and pressure-shear soft recovery friction experiments[9] are employed to study time-resolved friction. The configuration uses the framework of elastic plane wave analysis to simplify the interpretation of the experimental results. However, the experimental procedure is tedious and complex. These experiments can simulate local conditions of pressure and slipping velocities occurring in high-speed machining applications. In the pressure-shear friction experiment, the impact faces are never perfectly parallel at the moment of impact. This feature implies that the normal and shear waves generated in the flyer and the target are inclined with respect to the free surface of the target plate where the motion is being measured. This effect produces a transient through the specimen. Such behavior leads to an elaborate data reduction procedure.[7] Furthermore, the high pressure introduced at the interface is such that substantial initial damage can be generated in brittle materials before sliding occurs, changing the surface properties under examination.
- The modified split Hopkinson bar method,[10] in which a dynamic axial force is applied to a rotating bar/specimen system, can be used to investigate kinetic friction under impact loading. To understand the dynamic contact of two bodies with initial velocities, the corresponding reactions must be evaluated independently. This experimental technique allows one to study the kinetic friction coefficient for periods of 10 to 20 μs, and the contact time is partially insufficient before the onset of sliding to generate a strong

H. D. Espinosa is an Associate Professor, A. Patanella is a Graduate Student and M. Fischer is a Graduate Student, School of Aeronautics and Astronautics, Purdue University, West Lafayette, IN 47907-1282.

Original manuscript submitted: July 21, 1999.
Final manuscript received: November 18, 1999.

adhesion over the contact surfaces. The technique does not represent the conditions found in many applications in which a steady normal pressure is applied and a tangential force appears dynamically at the interface. Using this technique, Ogawa[10] found that the kinetic friction coefficient in a wide sliding velocity range is nearly constant independent of the normal applied force, which contradicts the findings reported by Anand,[11] Anand and Tong[12] and Madakson.[13] The Kolsky bar apparatus was also used by Feng and Ramesh[14] in the study of lubricants.

- Pin-on-disk tests[15] are designed for low-velocity friction experiments in which the kinetic friction is evaluated only in the steady-state condition. Researchers use pin-on-disk tests to study the mechanisms involved in the degradation of material surfaces in contact for long periods of time. This configuration does not allow for the study of the early frictional mechanism and the original surface deformation over the contact area due to the cyclic stressing of the tribo-components. The continuous contact of the two materials under study generates a permanent friction heating that degrades the original surface characteristics, resulting in difficulties in the interpretation of the obtained data. This experiment also depends significantly on the stiffness of the pin contacting the disk to prevent any vibration-induced effect in the tribo-system, which leads to a completely different frictional behavior.
- Various other techniques, ranging from quasi-static conditions to very low sliding velocities, are primarily used for studying quasi-static frictional behavior. Most are designed for a specific purpose and generally provide data only for the tribo-system for which they were designed.[16]

These techniques address the response of surfaces as encountered in real applications. Note that friction is a macroscopically observable phenomenon containing multiscale information. In this regard, the study of friction at the atomic scale is relevant to provide insight into the physics of interfacial forces. However, such study needs to be linked to the macroscopically observed friction phenomenon through a suitable model.

In this paper, we address the friction behavior at the macroscopic scale on surfaces that are contaminated by their interaction with the environment. We present the design of a modified Kolsky bar apparatus,[17] suitable for the investigation of dynamic friction at sliding velocities between 1 and 7 m/s, and contact area pressures in the range of 50 to 200 MPa. The experimental methodology and the formulas used to interpret the experimental data are presented. A discussion of the time evolution of interfacial friction in several material pairs is provided. The materials include Al 6061-T6, Ti-6Al-4V, 1080 steel and SAE 4340 steel, as well as those used as machining tools, such as WC/Co (cermet) with 11 percent of Co.

Dynamic Friction Experiments

Stored-energy Kolsky Bar

Several investigators have contributed to the development of the torsional Kolsky bar, originally designed by Kolsky.[18,19] Duffy *et al.*[20] used explosive loading to initiate the loading pulse. By combining outputs from the strain gages on either side of the specimen and by integration of the strain rate versus time, a complete record of the stress-strain curve can be obtained easily and accurately.[20] The explosive loading has the advantage of producing the shortest possible pulse rise time. Alternatively, a stored-torque loading system provides fast rising pulses.[20,21] This last configuration was the one chosen in the design of our dynamic friction experimental technique.

A stored-energy Kolsky bar, shown schematically in Fig. 1, was designed and built to investigate dynamic friction and compression-shear material behavior with specimen recovery. It is composed of two 1 in. (25.4 mm) 7075-T6 aluminum alloy bars. The incident or input bar is 90.5 in. (2.3 m) long, and the transmission or output bar is 75 in. (1.9 m) long. Each bar is supported along its length and aligned properly. They are supported by a series of recirculating ball fixed-alignment bearings (INA KBZ16PP) that minimize the friction resistance at the supports and allow the bar to rotate and translate freely in both directions. The distance between two consecutive supports is adjustable to prevent buckling. The compression or tension and shear loading pulses are produced by the sudden release of the stored elastic energy in the incident bar, which requires both torsional and compression/tension actuators. The axial part of the elastic energy is produced by means of a hydraulic double-acting actuator (Enerpac RD 166), which applies a compressive or tensile load at one end of the incident bar. Its capacity is 35 kips (150 kN). The torsional part of the elastic energy is achieved by means of a hydraulic rotary actuator (Flo-Tork 15000-180-AICB-ST-MS2-RKH-N) located along the incident bar. It is connected to the bar by a 3/8 in. steel key. Its capacity is 15000 lb·in. (1700 N·m). Changing the relative distance of the rotary actuator and the clamp, the duration of the loading pulse can be adjusted up to 650 μs. The hydraulic actuators are pressurized by three hand pumps (Enerpac P-84). The sudden release of the stored energy is achieved using a C-clamp positioned between the rotary actuator and the specimen.

The design of the C-clamp is crucial for good results. The C-clamp must be able to hold the desired torque and compression or tension force without slippage and release the stored energy fast enough to produce a sharp-fronted stress pulse traveling toward the specimen. Some changes were done to the C-clamp design discussed in Duffy *et al.*[20] However, it is similar to the C-clamp design discussed in Gilat and Pao.[21] The clamp consists of a vise mechanism, shown in Fig. 1. The vise faces are pushed against the incident bar by means of a hydraulic C-clamp with a capacity of 10 tons (Enerpac A-20 and Enerpac RC-125 single-acting actuator). Friction between the bar and the vise faces generates the load required to counteract the one applied by the hydraulic actuators. A notch in the pin, used to equilibrate the C-clamp load, is designed to fracture after the desired energy is stored and no sliding is registered in the clamp. The clamp vises are further pressed in a way that the notched pin fractures, releasing the stored energy. This clamping technique enables the application of large amounts of energy while avoiding slippage of the bar. The same principle is used when friction experiments are conducted in which the axial load is applied statically, before arming the clamp.

For the case of axial dynamic loading, the gripping force of the clamp balances the applied axial force. To prevent the generation of bending waves, an axial load support in contact

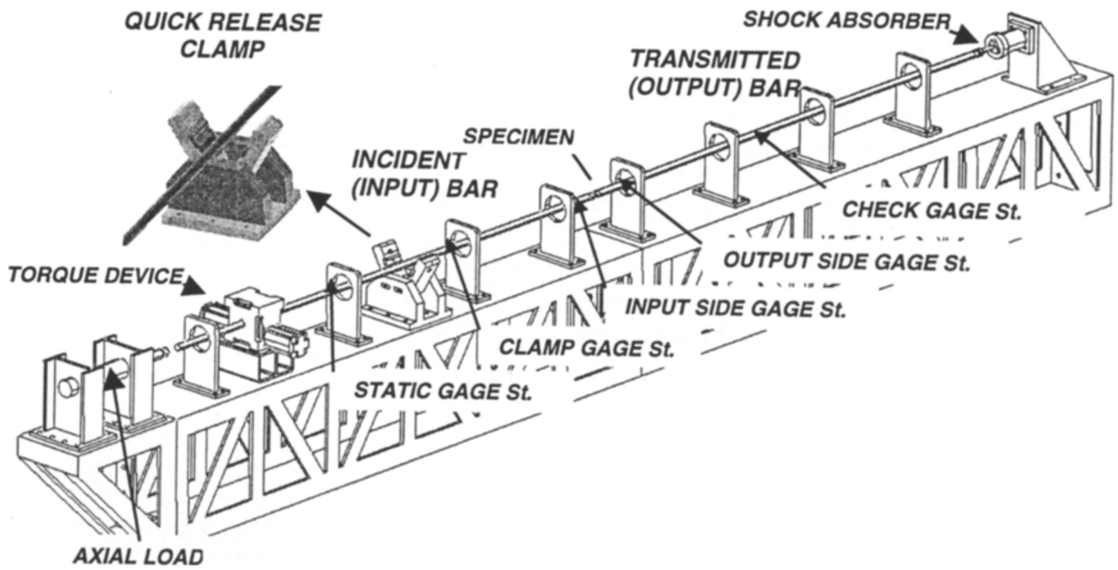

Fig. 1—Schematic of the stored-torque torsional Kolsky bar apparatus. Each station has a full strain gage bridge arrangement to measure torsional loads (with an alignment of 45 deg with respect to the longitudinal axis of the bar) and axial loads (aligned parallel to the longitudinal axis of the bar), except the bending station (half bridge), which monitors the presence of any spurious bending wave transmitted through the specimen

with the clamp faces is used to equilibrate the axial load applied to the clamp. The contact is made so that it allows both clamp parts to open with minimum resistance and absence of clamp bending. The point of contact is in a horizontal plane that contains the bar axis. In this way, no bending moment is transferred to the loading pulse due to misalignment of the clamp when the axial loading is applied. This device is added to the standard clamp configuration when a combined state of load is required. The C-clamp is supported from above by a cable and pulley arrangement to minimize the possibility of applying an external load other than the reaction to the stored load. It also allows the C-clamp to be positioned with high accuracy within the clamp assembly.

The amount of energy required to achieve the desired strain rate or sliding velocity is a determining factor in selecting the notched-pin material and the depth of the notch. Pulse rise time is also affected by the choice of the material for the notched pin. The pin must show a minimal ductility but be able to prevent the fracture before the clamp is tightened to ultimate load. The choice made for the pin material is aluminum 6061-T6. The clamping force determines the depth of the notch and fracture load required. For the purpose of dynamic shear studies, a 0.5 in. notch is used. Some researchers have used steel pins, but even brittle steels produce longer rise times than do aluminum alloys.[20]

In the case of friction experiments, the axial load is applied before gripping the clamp; that is, the friction phenomena are studied under static pressure conditions and a torsional pulse, resulting in a given amount of angular velocity. A Lagrangian X-t diagram, showing the elastic shear wave fronts, is shown in Fig. 2. Upon release of the clamp, a torsional pulse with constant amplitude equal to half of the stored torque propagates down the bar toward the specimen. Simultaneously, an unloading pulse of equal magnitude propagates from the clamp toward the rotary actuator. The torsional mechanical impedance of the rotary actuator is sufficiently large that after reflection, the unloading wave reduces the torque in the incident bar to zero as it propagates back along the bar. This was verified in the characterization and calibration process of the bar.[17] The duration of the loading pulse is the time required for the pulse to travel twice the distance along the bar between the C-clamp and the torsional actuator. The configuration used in our tests is set to a 290 μs loading pulse.

As the torsional pulse travels down the bars, it is detected by two strain gage stations, one on the incident bar and another on the transmitted bar. The axial pulse is detected by two stations, one on each bar. In the case of a static axial load, the gage station on the incident bar is used for measuring the axial load applied to the interface and to check that no axial pulse exists when the clamp is released. The station in the transmitted bar is used to interrogate the appearance of any bending wave or other spurious loading. Each station consists of a full bridge arrangement of four strain gages of 350 Ω (MM EA-13-250BF-350) bonded using a cyanoacrylate-based glue (MM M-Bond 200) and protected with a polyurethane coating (MM M-Coat A). The bridges are energized with 16 VDC regulated power supply (Calex 460-220).

The apparatus described here is conceptually simpler than the one discussed by Ogawa[10] and can easily be obtained through modification of the traditional Kolsky bar available at many research laboratories. Moreover, the apparatus can be used to study shear instabilities and dynamic failure of advanced materials when compressive or tension and shear pulses are applied.

Formulas for Dynamic Friction Coefficient Calculations

The Lagrangian X-t diagram of the compression/torsion bar is shown in Fig. 3. The longitudinal and torsional elastic wave fronts along the bar are shown. This wave diagram is used in dynamic torsional studies with specimen

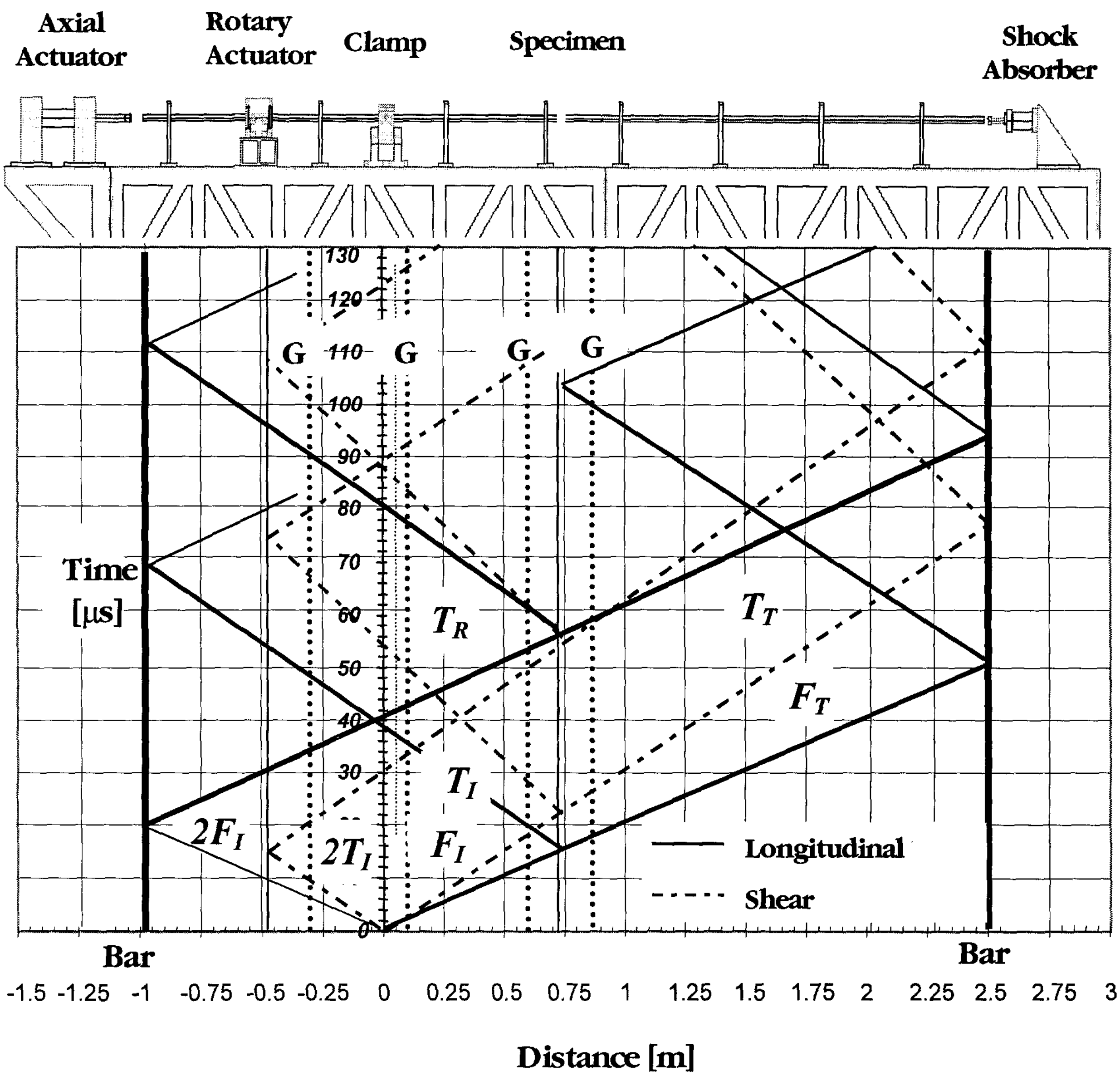

Fig. 2—Lagrangian X-t diagram showing shear wave fronts, gage stations and points 1-8 used in characteristics analyses

recovery. Upon release of the clamp, two waves, longitudinal and shear, are propagated toward the specimen and toward the hydraulic actuators. The length of the bars and the position of the actuators are selected such that the incident shear pulse duration can be transferred to the transmission bar before momentum trapping caused by the arrival of an unloading wave to the specimen from the right-hand end of the transmission bar. This trapping concept is identical to the one used by Clifton and Kumar[22] in the study of plate impact with specimen recovery. It should be noted that because the specimen is sleeved to the transmission bar, tensile loading leaves the specimen free to translate and rotate due to the effect of the reflected waves trapped in the incident bar. The same wave propagation history can be used in dynamic friction experiments. However, another possibility is to apply quasi-statically the axial stress and equilibrate only torsional energy as discussed earlier.

The X-t diagram, shown in Fig. 2, describes the dynamic frictional test when a uniform quasi-static contact pressure, obtained by applying an axial force by means of the axial actuator, is applied instead of the longitudinal pulse. This static pressure is applied to the sample before the clamp starts to store the torsional energy. The reason for selecting this loading procedure is that in this case the clamp needs to equilibrate only the torque. As a result, large-amplitude torsional waves and, consequently, large sliding velocities can be obtained. A disadvantage is that the specimen is not subjected to single pulses, although in practice we observed that only the main torque is strong enough to achieve sliding. The specimen geometry is shown in Fig. 4. It is composed of two disks, one of which has a hollowed end.

Based on the above description of precompression, elastic torsional waves and measurement stations, we can infer that the shear frictional stress in the contact area of the sample is given by

$$\tau_s = \frac{T_T \cdot r}{J_{ps}}, \qquad (1)$$

where T_T is the transmitted torque (measured at gage station G3), J_{ps} is the contact area polar moment of inertia and r is the centerline radius.

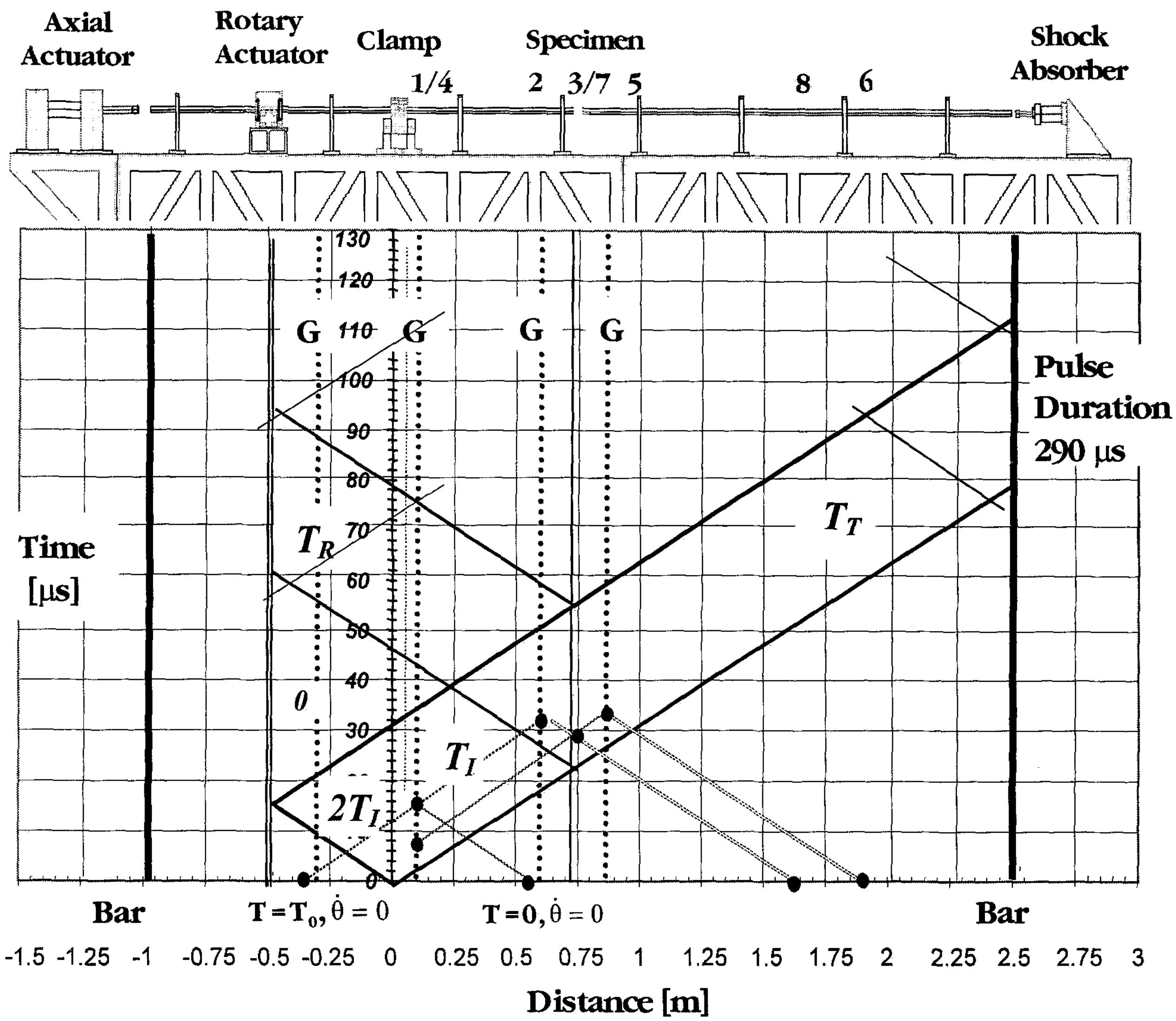

Fig. 3—Lagrangian X-t diagram showing longitudinal and shear wave fronts for the case of pressure-shear recovery experiments

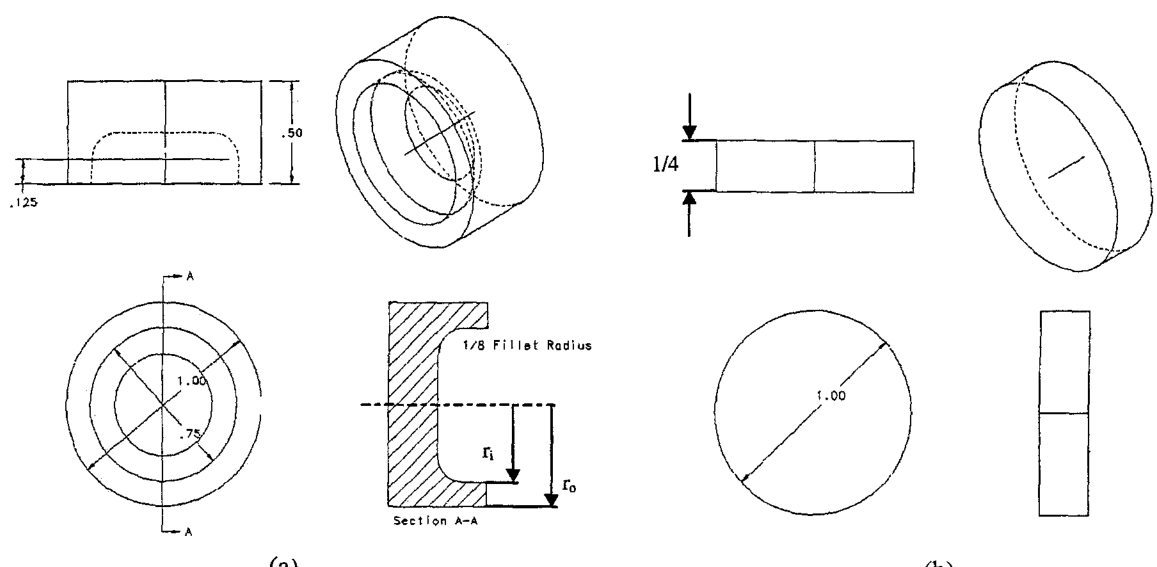

Fig. 4—Friction specimen: (a) U-shaped disk attached to the incident bar, (b) disk attached to the transmission bar

The angular velocities of the input and output bars represent the angular velocities at the contact surfaces. For elastic bars, the wave propagation phenomenon can be described by the following characteristic equations:

$$T \pm \rho C_s J_P \dot{\theta} = \text{ constant along } \frac{dx}{dt} = \pm C_S, \quad (2)$$

where T is the torque, C_s is the shear wave speed in the bar, ρ is the material density, J_p is the polar moment of inertia and $\dot{\theta}$ is the angular velocity. By placing gages at stations G1 through G3, the sliding velocity history and shear stress history at the sliding interfaces can be obtained. To see this, consider point 1 in the X-t diagram. From the initial conditions in the bar, we find that $T_1 = T_0/2$, where T_0 is the stored torque. Furthermore, the angular velocity at point 1 is $\dot{\theta}_1 = -T_1/(\rho C_s J_P)$. Similarly, for point 4, $T_4 = T_0/2$ and $\dot{\theta}_4 = -T_4/(\rho C_s J_P) = -T_1/(\rho C_s J_P)$.

By considering points 1-2-3-4, it can be shown that $T_2 = T_3$ and $\dot{\theta}_3 = (T_2 - T_0)/(\rho C_s J_P)$. Similarly, considering points 5-6-7-8, we find that $T_5 = T_7$ and $\dot{\theta}_7 = -T_7/(\rho C_s J_P)$. The rotation jump is given by

$$\dot{\theta}_3 - \dot{\theta}_7 = \frac{T_2 + T_5 - 2T_1}{\rho C_S J_P}. \quad (3)$$

Note that $T_1 = T_I$ is the input torque measured at station G_1. Moreover, $T_5 = T_T$ is the transmitted pulse measured at station G_3. Finally, T_2 is the torque measured at gage station G_2. This station is close to the specimen but outside the region in which bar end effects are present. From a practical standpoint, it is customary to place G_3 symmetrically to G_2 about the specimen. Note that in the analysis above, no assumptions are made about the continuity of traction at the sliding interfaces. Only the information measured at the gage stations is required to compute the history of friction. If we assume continuity of traction,

$$T_I - T_R = T_2 = T_T = T_5, \quad (4)$$

then

$$\dot{\theta}_3 - \dot{\theta}_7 = \frac{2T_T - 2T_1}{\rho C_s J_P} = \frac{2(T_1 - T_R) - 2T_I}{\rho C_s J_P} \quad (5)$$

$$\dot{\theta}_3 - \dot{\theta}_7 = -\frac{2T_R}{\rho C_s J_P}. \quad (6)$$

In general, the average sliding velocity over the contact area is given by

$$\nu_r = \frac{\int_{ri}^{ro} r^2(\dot{\theta}_3 - \dot{\theta}_7)dr}{\int_{ri}^{ro} r dr}, \quad (7)$$

where r_o and r_i are the outer radius and inner radius of the specimen contact area, respectively. Solving the integrals, a relation between the average sliding velocity and the reflected torque is obtained, that is,

$$\nu_r = \frac{2}{3}\frac{\left(r_o^2 + r_o r_i + r_i^2\right)}{(r_o + r_i)}(\dot{\theta}_3 - \dot{\theta}_7). \quad (8)$$

Furthermore, replacing the values of $\dot{\theta}_3$ and $\dot{\theta}_7$ obtained from the reading of the torques in each gage station, and if the transmitted pulse is expressed as the difference between the incident and the reflected pulses ($T_T = T_I + (-T_R)$), the average sliding velocity becomes

$$\nu_r = \frac{2}{3}\frac{\left(r_o^2 + r_o r_i + r_i^2\right)}{(r_o + r_i)}\frac{2T_R}{J_P \rho C_s}. \quad (9)$$

The validity of the expression ($T_T = T_I + (-T_R)$) was verified experimentally by measuring each torque independently.[17]

The relative average displacement between the surfaces in contact can be determined from eq (9) upon integration as

$$S = \int_0^t \nu_r dt, \quad (10)$$

where t is the duration of the loading pulse.

The normal stress in the contact area is determined by the static pressure applied to the specimen by means of the axial hydraulic actuator. The axial load (N_I) is measured by the strain gage station located before the clamp. The macroscopic normal stress is directly computed as

$$\sigma_s = \frac{N_I}{A_c} = \frac{N_I}{\pi(r_o^2 - r_i^2)}, \quad (11)$$

where A_c is the contact area.

The shear stress is computed by means of elastic wave propagation theory, as is the case in shear dynamic strength studies. Replacing the value for the polar moment of inertia of the sample in eq (1), we obtain

$$\tau_s = \frac{2T_T r}{\pi(r_o^4 - r_i^4)}. \quad (12)$$

Then, the shear stress averaged over the contact area can be expressed by

$$\tau_a = \frac{\int_{ri}^{ro} r\tau_s dr}{\int_{ri}^{ro} r dr} \quad (13)$$

$$\tau_a = \frac{2}{3}\frac{\left(r_o^2 + r_o r_i + r_i^2\right)}{(r_o + r_i)}\frac{2T_T}{\pi\left(r_o^4 - r_i^4\right)}. \quad (14)$$

At this point, all the variables needed to compute the friction coefficient μ are defined. This coefficient, representative of a steady-state sliding velocity, is given as $\mu = \tau_a/\sigma_n$.

The above formulas provide a direct measurement of the quasi-static and kinetic frictional properties by using load (strain) histories detected at the output and input bars.

Experimental Procedure

A static axial load is applied before the clamp is pressed to equilibrate the torsional load. In this way, the surfaces of the pair of materials to be tested are prestressed with a known pressure. It is very important that the surfaces in contact represent an annulus with small thickness, where the torsional stress profile can be assumed to be constant, resulting in an almost constant profile of relative sliding velocity along the radial direction. For this reason, a geometry such as the one shown in Fig. 4 was chosen.

Before clamping the incident bar, it is necessary to check that the pressure along the contact area is uniform. This important variable in the experiment needs to be verified using a nondestructive method to avoid altering the characteristics and cleanness of the surface. The simplest method that meets all these requirements is the use of pressure-sensitive film. A Fuji prescale pressure measurement film was used. The pressure in the contact area is usually greater than 10 MPa, so a medium pressure scale film is used ranging from 10 MPa to 50 MPa. A sample pattern obtained from an experiment is shown in Fig. 5. The shaded ring represents the contact area, and the grade of the shade represents the pressure in that interface. The pattern shown is quite uniform. The same uniformity is kept in all the experiments. If the pressure pattern is nonuniform, the samples have to be reglued to the bars or lapped further until a uniform pattern is achieved.

To ensure flatness and parallelism of their surfaces, each sample was lapped before each test in a Lapmaster 24 lapping machine from Crane Co. Silicon carbide powder of 12.5 μm was employed. The specimens were cleaned using MEK, acetone and alcohol in an ultrasonic bath for 30 min. Through this surface preparation procedure, it is expected that a few nanometer thick oxide layers and contaminant films will be present from interaction of the surface with the environment. For a discussion of chemical species and surface analysis techniques, see Miyoshi[23] and references therein.

Marking of the sample was performed to allow the study of surface changes in the area surrounding the mark after the experiment. The objective was to identify the friction mechanisms in the pair of materials tested.

To analyze the surface properties, an AFM from Digital Instruments (Dimension 3100A model) was used. On each tested sample, an area of approximately 50 μm by 50 μm, about 50 μm from the mark, was scanned. The surface profile, a three-dimensional micrograph and the average roughness height, in that area, were taken from each scan in each sample.

Fig. 5—Pressure distribution along the contact area as recorded by pressure-sensitive film

The most important values taken from the roughness analysis were the root mean square roughness (R_q) and the average roughness height (R_a). It can be argued that for some surfaces, these parameters are scale independent in the sense that changes in statistical sample size or instrument resolution do not lead to different values. For details on surface roughness characterization, the use of fractal techniques and a discussion of how these measurements can be used in the formulation of mathematical models, see Majumdar and Bhushan.[24] In the section analysis, the most important features are the profile of the section and the maximum distance between valleys and peaks. The section profile is taken along the sliding direction. All these parameters are measured again after the experiment to examine the amount of roughness change and to infer the friction mechanisms present in the test.

After the specimen is glued, the pressure distribution on the contact area checked and the surfaces cleaned, the test is conducted. The cleaning is performed using MEK, acetone and methanol to eliminate any chemical residue.

The contact pressure is set to the desired value by means of the axial load actuator. Then, the C-clamp is closed and the torque stored to give the desired sliding speed. After releasing the stored energy, by breaking the clamp pin, the signals are recorded in the oscilloscope using the incident pulse signal raise ramp to trigger the scopes. A typical recording is shown in Fig. 6.

Experimental Results and Discussion

Several experiments were conducted to study the frictional behavior of different material pairs. For instance, aluminum 6061-T6 (RB 97) and steel SAE 1018 (RB 89), titanium Ti 6Al 4V (RC 33) and steel SAE 1018 (RB 89), aluminum 6061-T6 (rough) (RB 97) and aluminum 7075-T6 (mirror polished) (RB 61), aluminum 6061-T6 (rough) (RB 97) and aluminum 7075-T6 (rough) (RB 61), titanium Ti 6Al 4V (RC 33) and WC/Co 11 percent (RC 78), and SAE 4340 (RC 45) and WC/Co 11 percent (RC 78).

The first four pairs were used to verify the new experimental technique.[25] The last two pairs were used to investigate the sliding velocity dependence of the frictional behavior and to extend Prakash and Clifton's[7] plate impact work. A summary of experimental results is given in Tables 1 and 2. In each set of experiments, the average sliding velocity was kept on the order of 2 to 5 m/s. The data are presented taking the average value found in each particular set of experiments. The computed standard deviation is given in parentheses. The scatter found in the data can be attributed to the many variables involved in the experiment, but after several experiments a trend can be predicted for each pair. The deviation falls on the order of 10 percent, which is acceptable for engineering applications. Moreover, the quasi-static friction coefficients measured are in agreement with data reported by different investigators using other test methods.

A typical time-resolved friction coefficient is shown in Fig. 7 for the Al 6061-T6–Steel 1080 material pair. A 10 moving point average was added to the data-processing procedure to reduce the oscillations produced by data noise. Note that no amplification or filtering is done to the original signal. This curve is obtained by processing the raw data shown in Fig. 6 using the theoretical analysis presented earlier. The formulas were programmed using the Excel '97

TABLE 1—EXPERIMENTAL RESULTS FROM FRICTION STUDIES ON METALS

Materials Pair	Sliding Velocity [m/s]	Contact Pressure [MPa]	R_q [nm]	μ_s	μ_k
Al 6061-T6 (RB 97)			$479.24^{(84.19)}$		
Steel 1080 (RB 89)	$3.11^{(0.68)}$	$37.58^{(10.4)}$	$504.39^{(122.2)}$	$0.421^{(0.071)}$	$0.33^{(0.077)}$
Ti 6Al-4V (RC 33)			$441.91^{(86.79)}$		
Steel 1080 (RB 89)	$3.375^{(0.35)}$	$35.99^{(5.5)}$	$472.82^{(65.15)}$	$0.35^{(0.044)}$	$0.259^{(0.053)}$
Al 6061-T6 (RB 97)			$529.49^{(89.04)}$		
AL7075-T6 (mirror) (RB 61)	$3.457^{(0.73)}$	$43.42^{(8.57)}$	$27.12^{(3.26)}$	$0.405^{(0.049)}$	$0.418^{(0.057)}$
Al 6061-T6 (RB 97)			$466.51^{(51.39)}$		
Al 7075-T6 (rough) (RB 61)	$3.22^{(0.43)}$	$34.918^{(3.5)}$	$441.58^{(46.94)}$	$0.466^{(0.049)}$	$0.342^{(0.074)}$

Standard deviations in parentheses

TABLE 2—FRICTION BEHAVIOR OF HARD-TO-MACHINE MATERIALS AND A WC/Co TOOL MATERIAL

Material Pair	Contact Pressure (MPa)	Sliding Velocity (m/s)	Friction Coefficient (μ)	Reference
	31.95	Static	0.478	E-P-F
	28.061	Static	0.49	E-P-F
	28.91	Static	0.4	E-P-F
	28.135	Static	0.49	E-P-F
	2010	2.9	0.233	P-C
	28.061	3	0.28	E-P-F
SAE 4340	28.91	3.4	0.25	E-P-F
-	28.135	3.7	0.21	E-P-F
WC/Co 11 percent	1910	4.83	0.223	P-C
	3058	6	0.25	P-C
	2384	7.73	0.221	P-C
	1340	11	0.157	P-C
	1718	14.39	0.148	P-C
	2520	17	0.21	P-C
	2046	17.43	0.132	P-C
	40.01	Static	0.36	E-P-F
	39.01	Static	0.41	E-P-F
	37.64	0.9	0.33	E-P-F
Ti-6Al-4V	1590	1.35	0.255	P-C
	1575	1.38	0.25	P-C
WC/Co 11 percent	39.01	2	0.31	E-P-F
	40.01	3.4	0.24	E-P-F
	1715	6.17	0.232	P-C
	1820	11.2	0.22	P-C
	1576	12.93	0.168	P-C

P-C: Prakash and Clifton[7]
E-P-F: Current study

software from Microsoft in order to make the data reduction process automatic.

A couple of features can be pointed out from the friction coefficient time-evolution shown in Fig. 7. Two peaks in the friction coefficient are found. They mark the beginning and the end of the pulse where the sliding velocity is rising from zero to sustain a constant value and then falling to the rest condition again. Due to this behavior, the first peak represents the static coefficient of friction (μ_s) and, after a transient time, the sliding velocity remains constant, providing a measure of the kinetic friction coefficient (μ_k). At the end of the pulse, the sliding velocity goes to zero and the coefficient of friction rises again toward a value corresponding to μ_s. This second value of μ_s is expected to be lower than the first one due to the changes on the sliding interfaces by the previous loading. Sometimes, no second peak is found as a function of material pair and surface roughness. A plausible explanation is that the amount of plasticity generated on the surfaces reduces the surface roughness in such an amount that the static coefficient is significantly reduced. Moreover, frictional heat may result in material softening. The frictional response can be explained by studying the sliding process in detail.[13] When the tangential load is applied, a first elastic deformation of the asperities and the substrate takes place. It continues until the shear strength of the junctions is reached. Shearing of the junctions now takes place, and the coefficient falls off as the strong junctions, which were formed during static loading (initial pressure), are replaced by weaker ones. The influence of the strong junctions persists over a distance that is simply related to the average junction size. That behavior is strongly affected by the strain rate and temperature sensitivity of the material under study. Some models were developed to relate all the material properties to the friction phenomena. However, many of them fail under certain conditions.

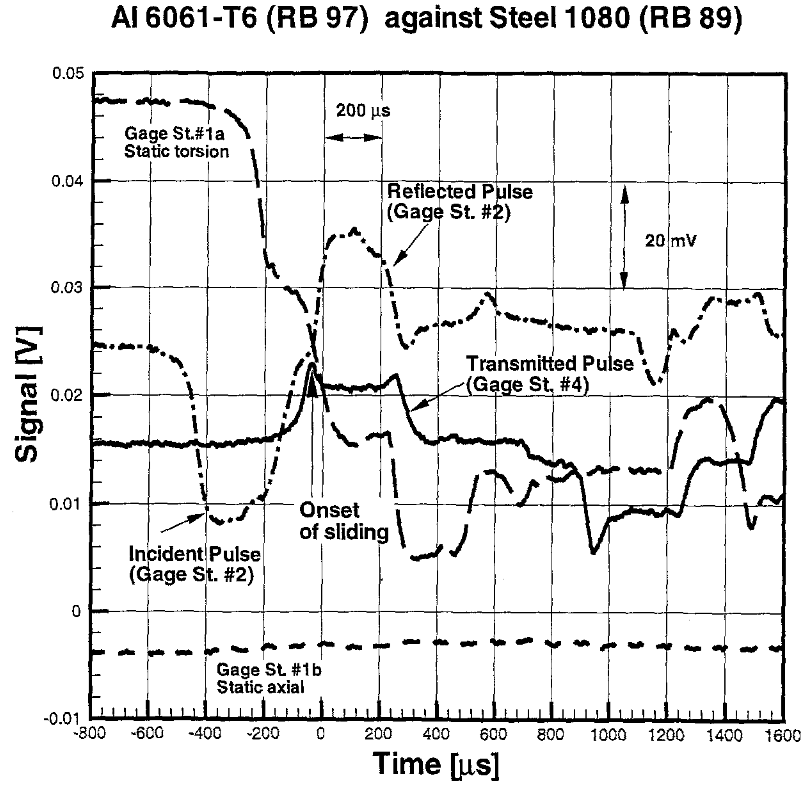

Fig. 6—Recorded raw data at gage stations G1 through G4

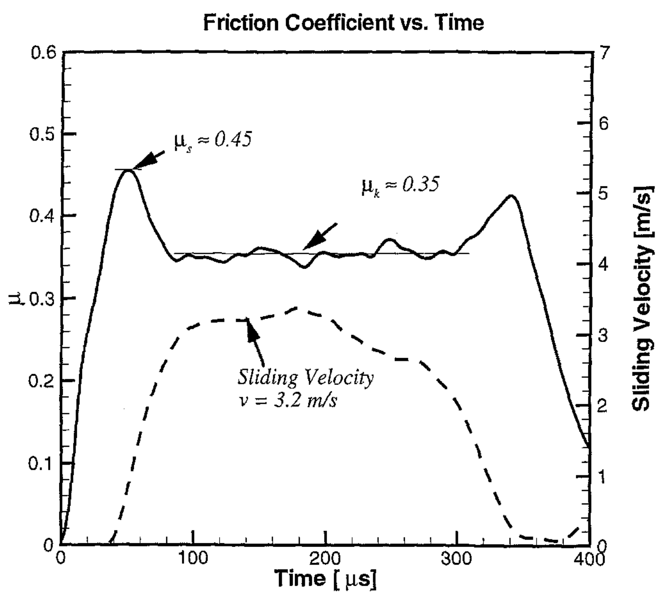

Fig. 7—Friction coefficient history

The link between the time-dependent plasticity and surface friction is difficult to establish due to the large number of variables involved in friction phenomena.[13,16] Some models have successfully incorporated material strain rate sensitivity on the prediction of the friction coefficient, as described by Brechet and Estrin.[26] These models may provide valuable tools for further understanding the experimental observations discussed here.

The actual area of contact between two solids in friction is only a small fraction of the nominal contact area.[27] The asperities in contact, forming a junction, deform elastically until the shear stress supported by each junction reaches the value of the material's yield stress. Then, the force necessary for sliding is determined by the stress needed to shear the junctions. In this context, the quasi-static friction coefficient is time independent. However, early experiments[28] showed that the quasi-static coefficient is time dependent. Moreover, it was suggested that this dependence is the very cause of the sliding velocity dependence of the dynamic friction coefficient. The aging of asperities is in part responsible for the decrease in friction coefficient with increasing sliding velocity. The average time for shearing of an asperity junction is inversely proportional to the imposed sliding velocity. This aging effect and, hence, the strength of the junctions diminishes with the increase in sliding velocity.

The effect of sliding distance on friction depends on the nature of the initial deformation of the rubbing surfaces, which is governed by the surface finish (roughness), normal load, sliding velocity, material properties and environmental conditions.[30,31] The first stage of friction, in which a quasi-static phenomenon is encountered, can be easily seen in the experimental data shown in Fig. 8. The effect of the breakdown of asperities and the role of material response can be observed in this plot. They basically correlate with sliding distance S'. This effect is significant when the elastic portion of the friction phenomena is taking place. After the plastic process starts, the surface is deformed enough to reduce the friction coefficient to the kinetic value.

The extent of plasticity found on the contact surfaces, on both sides of the contact area, is a function of the thermomechanical properties of the surfaces in contact, such as surface hardness and shear strength of each material. This can be seen by observing the surfaces of tested samples using atomic force microscopy.[25]

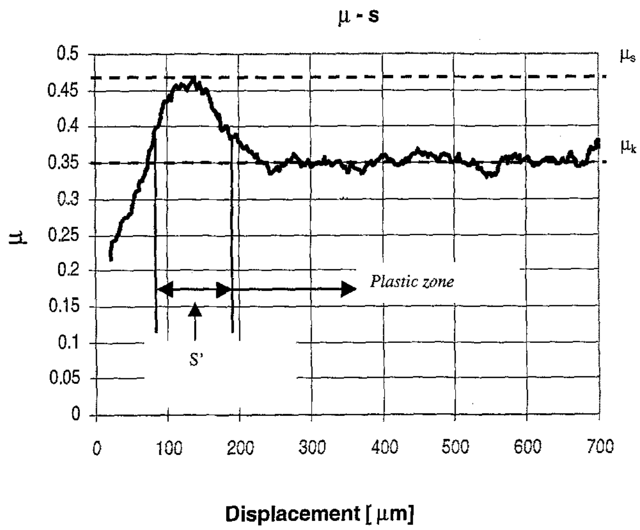

Fig. 8—Friction coefficient versus accumulated displacement curve

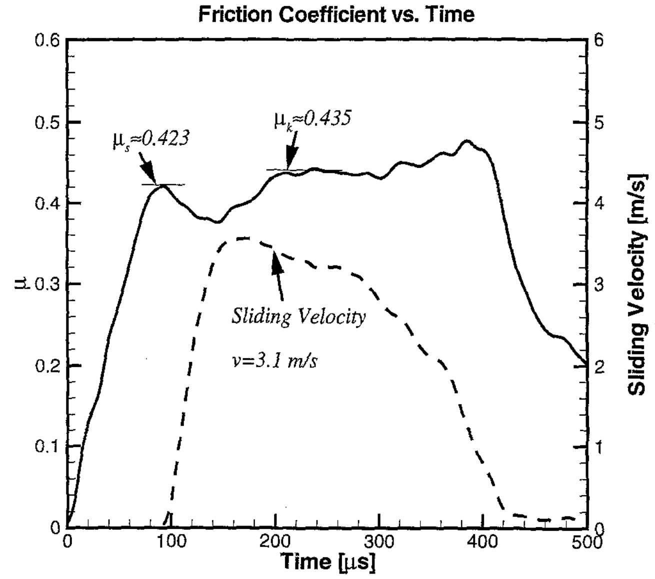

Fig. 9—Friction coefficient history for Al 6061-T6 sliding at 3.1 m/s on Al 7075-T6 mirror polished. Note the increase in friction coefficient with time

Insight into the variability of the friction coefficient reported in the literature can be obtained by examining the effect of surface roughness. The friction coefficient history measured in the Al 6061-T6–Al 7075-T6 pair is quite different from the one described in Fig. 7. In this case, one of the surfaces in contact was mirror polished. The friction history shows that the static friction coefficient is smaller than or almost equal to the kinetic friction coefficient. This behavior can be attributed to the lack of large enough asperities in the mirror-polished surface (as shown in Fig. 10), with an R_a on the order of 30 nm for the Al 7075-T6 disk. Asperities interlocking between surfaces in contact do not occur initially. However, when the mirror-polished surface becomes rough, during the sliding process, the interlocking phenomenon can be achieved, which slightly raises the value of the friction coefficient. This feature is clearly observed in the μ-time history shown in Fig. 9.

The generation of asperities on the mirror-polished Al 7075-T6 surface can be seen in the AFM surface analysis performed on the surfaces before and after the friction test (see Fig. 10). In addition, using optical microscopy, the surface roughness, introduced during the test, can be observed on a larger scale (see Fig. 11). In the case of the mirror-polished surface, many imprints are observed. These imprints are the origins of scratches generated when the sliding process starts raising the friction coefficient [see Fig. 11(a)]. The original rough surface shows almost no variation in morphology, and only a small reduction in roughness can be found. No deep scratches can be seen in the surface. The same behavior was found in all the samples studied in which one of the surfaces was mirror polished. When the same pair of materials is tested with both sides having similar roughness, the value of the static friction coefficient departs from the kinetic one ($\mu_s \approx 0.466$, $\mu_k \approx 0.342$ at 3.22 m/s, reported in Table 1). Moreover, the static friction coefficient is higher than the one encountered for the case discussed previously ($\mu_s \approx \mu_k \approx 0.41$ at 3.45 m/s). This change in the friction coefficient takes place because the friction mechanism changes when both surfaces are rough. The interlocking mechanism occurs on a larger number of contact spots, resulting in a higher μ_s. When the shear stress produced by the relative motion reaches a value close to the material flow stress, the asperities are plowed and sheared, reducing the frictional coefficient. This can be seen in the micrograph shown in Fig. 11(b). Here, no new asperities are generated. By contrast, some are eliminated. Both surfaces show a marked deformation with voids and scratches of the same magnitude. This example shows the importance of roughness and plasticity in the friction phenomena.

The last two sets of experiments were performed to complete the study started by Prakash and Clifton[7] on the effect of pressure and sliding velocity. They used the plate impact test to study the frictional phenomena of material pairs commonly used as machining tools or materials that are difficult to machine. They found the frictional properties at very high contact pressures and sliding speeds. However, the accumulated sliding distance was on the order of a few microns. This small sliding distance is the result of the short duration of the pulses. The plate impact friction experiment was later extended by Espinosa *et al.*[9] to achieve specimen recovery. Espinosa and colleagues verified that sliding marks of a few microns are produced on the sliding interfaces.

Using the modified Kolsky bar, the dynamic friction time response can be easily tracked for the entire loading pulse. Surface finishes similar to those of Prakash and Clifton[7] are used. The experimental results are reported in Table 2. The experimental values reported in Table 2 marked as P-C are reproduced from Prakash and Clifton.[7] When the sliding velocity is labeled as "static," it means the value corresponds to the static friction coefficient; otherwise, it corresponds to the kinetic friction coefficient.

In each set, the samples were lapped as described previously, and we obtained an average roughness of $R_a = 389$ nm ($R_q = 483$ nm) for 4340 steel, $R_a = 351$ nm ($R_q = 442$ nm) for Ti-6Al-4V and $R_a = 88.6$ nm ($R_q = 114$ nm) for WC/Co 11 percent. The friction coefficients reported in Table 2 can be plotted together to examine their dependence on sliding velocity (see Fig. 12). The friction coefficient decreases with increasing sliding velocity until it reaches a quasi-asymptotic level at sliding speeds above 10-12 m/s. It should be noted that the applied pressures in the plate impact and Kolsky bar

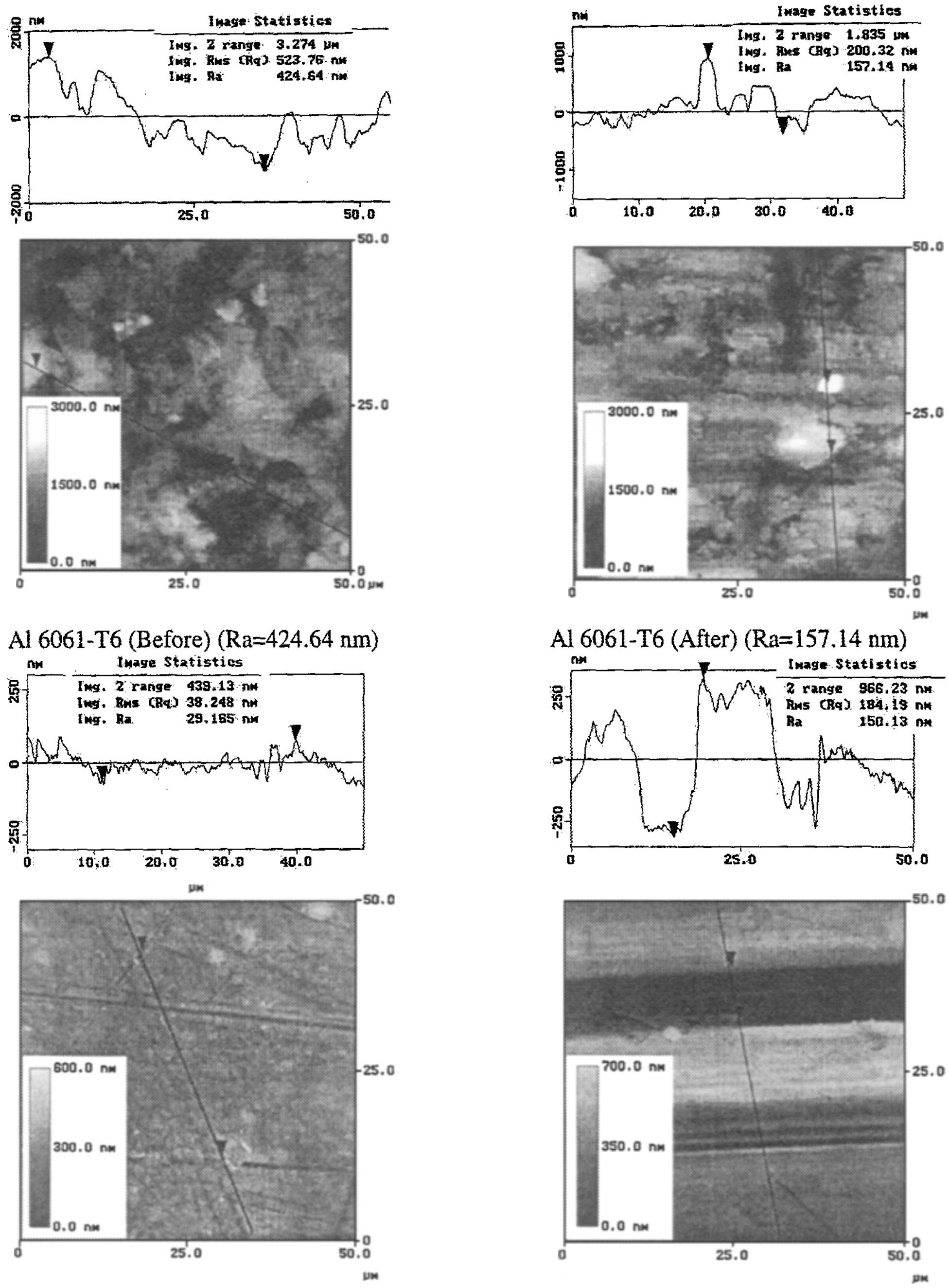

Al 6061-T6 (Before) (Ra=424.64 nm)

Al 6061-T6 (After) (Ra=157.14 nm)

Al 7075-T6 Mirror Polished (Ra=29.165 nm)

Al 7075-T6 Mirror Polished (Ra=150.13 nm

Fig. 10—Surface characteristics before and after the experiment. Al 6061-T6 rough sliding at 3.1 m/s against Al 7075-T6 mirror polished

tests differ on one order of magnitude. This may explain the lower kinetic friction coefficients measured by plate impact at sliding velocities of about 2 m/s.

Analyzing the surface features on the contact area, the WC/Co shows little change in its surface topography, and the softer materials, steel and titanium, show a marked change in their surface properties. Note that the sliding process in the Kolsky bar technique and the plate impact experiment is an almost adiabatic process due to the high velocity applied in the contact area and the short loading pulses. By examining the AFM micrographs shown in Figs. 13 and 14, the frictional behavior of the material pair can be inferred.

In the case of SAE 4340 steel sliding against WC/Co, the WC/Co surface shows an increase in roughness but not a significant change in surface topography. On the other hand, the SAE 4340 steel presents a reduction in roughness on the order of 50 percent and absence of deep scratches on the contact surface. In the case of Ti-6Al-4V sliding against WC/Co, the titanium alloy undergoes a surface roughness reduction on the order of 60 percent. Moreover, the surface shows more plastic work than the steel surface as evidenced by deep surface scratches. This seems consistent with the findings of other investigators. In fact, to machine titanium, low feeding velocities and low

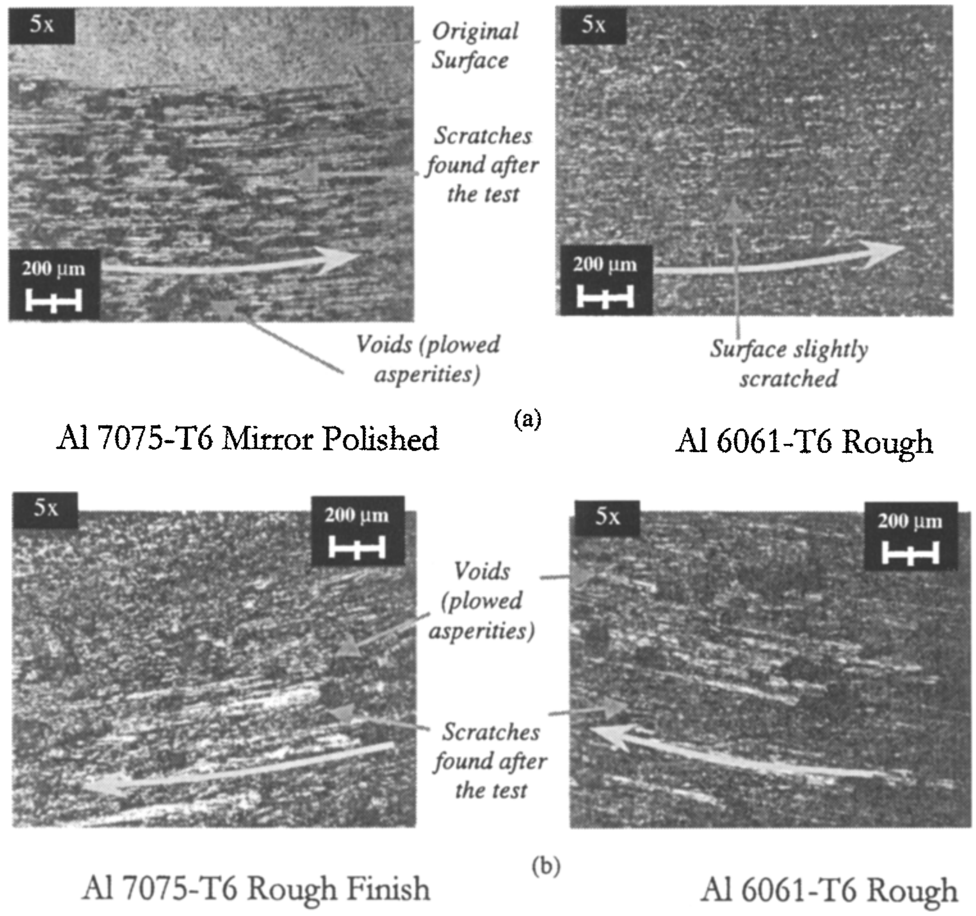

Fig. 11—Friction surfaces for Al 6061-T6 sliding against Al 7075-T6 mirror polished and rough finished (optical micrographs)

material/tool relative velocities must be applied to ensure a long life of the tool and a better surface finish of the work piece. This is due to the change in flow stress and hardness on the surface of the titanium alloy with the increase in local temperature without significant changes in bulk material properties. In the present experimental technique, the effect of frictional heat on changes in surface properties is difficult to assess because surface temperature measurement was not performed. Another feature to be mentioned is that WC/Co presents no major difference in surface topography for the two materials studied. Considering their wear resistance, WC/Co tools possess good properties for machining of materials.[32]

Concluding Remarks

A novel dynamic friction experiment using the Kolsky bar concept was developed. The technique is complementary to the plate impact and other macroscopic friction experiments in the sense that sliding velocities and pressures not attainable otherwise can be investigated.

The experimental results reported in this paper show that the technique provides accurate and repeatable measurement of time-resolved friction. The apparatus is simpler and easier to operate than the plate impact facility. However, it cannot achieve the same level of contact pressure and sliding velocity.

In the experiments discussed here, a precompression is applied prior to the dynamic torque. Other possibilities exist if single pulses are desired to guarantee specimen recovery with the specimen subjected to a single pulse. In fact, simultaneous storage of an axial force and a torque leads to a compression wave followed by a torsional wave. Total wave trapping in the transmission bar is then achieved, and the specimen is subjected to a single compression-shear pulse. The limitation of this approach is that the C-clamp can store less torsional energy, and therefore smaller sliding velocities can be studied.

Due to the importance of heating in the frictional properties of metals, future work should focus on the measurement of temperature history at the sliding interfaces. For that purpose, infrared photography appears to be a promising tool.

Many parameters must be varied to study the frictional behavior of rough surfaces. Various combinations of sliding velocity, pressure and surface roughness need to be tested for the formulation of accurate friction models. The parameters in the experiments conducted here were kept in a narrow range in order to investigate the repeatability of the measurements. In this way, the obtained data could be compared with data reported in the literature. In-depth frictional studies in advanced materials will be reported in future publications.

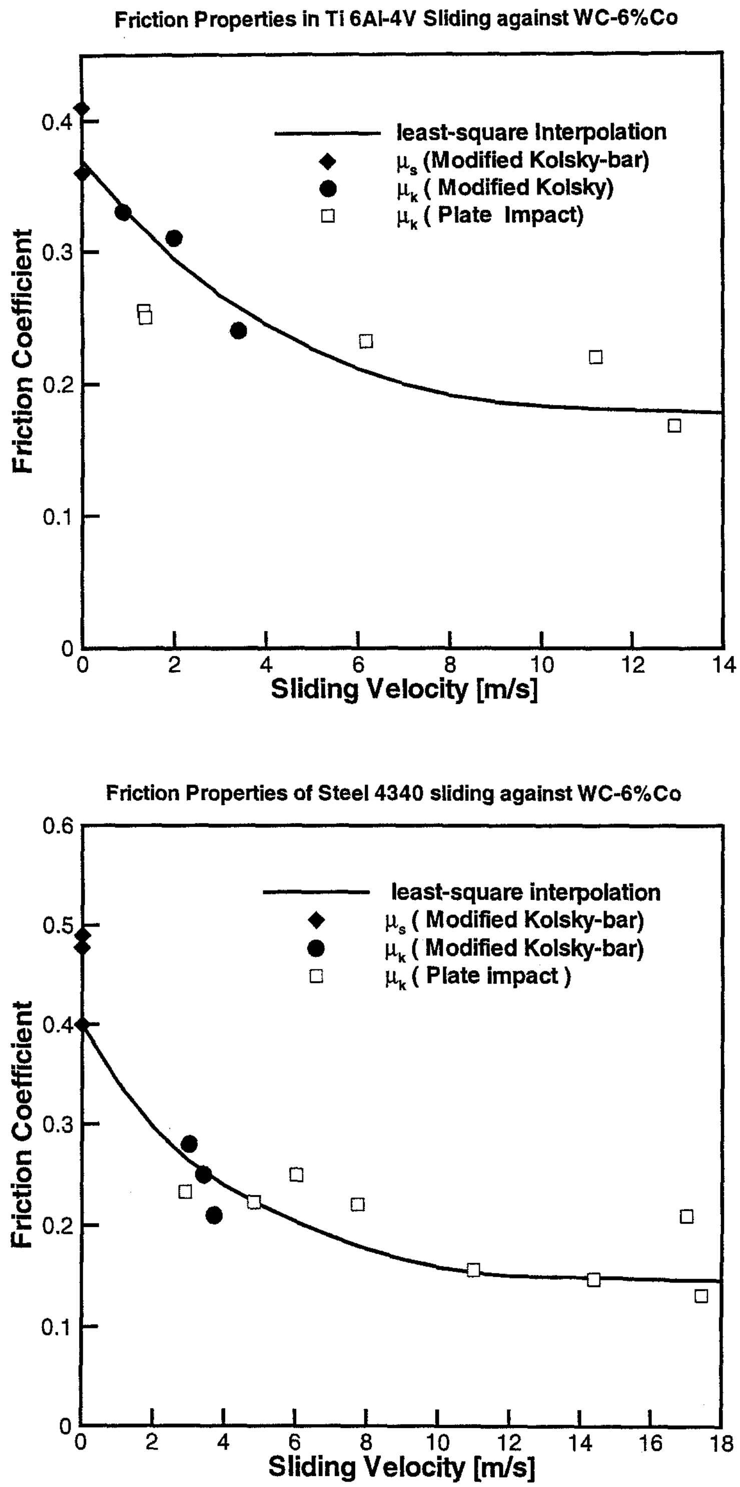

Fig. 12—Friction properties of SAE 4340 steel sliding against WC/Co and Ti-6Al-4V sliding against WC/Co as a function of sliding velocity

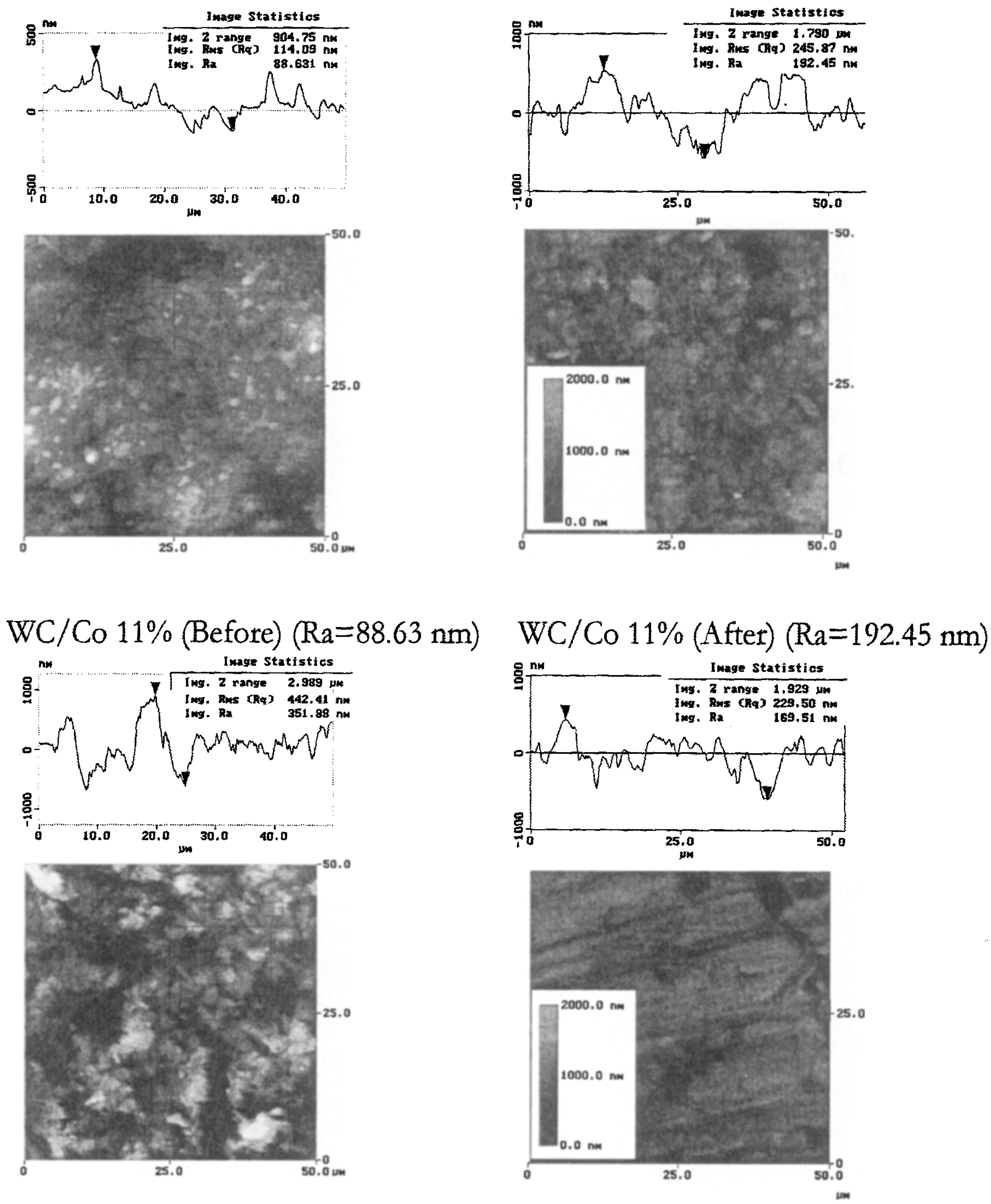

Ti 6Al-4V (before) (Ra=351.88 nm) Ti 6Al-4V (after) (Ra=169.51 nm)

Fig. 13—Atomic force microscope surface analysis of Ti-6Al-4V sliding at 2 m/s against WC/Co 11 percent

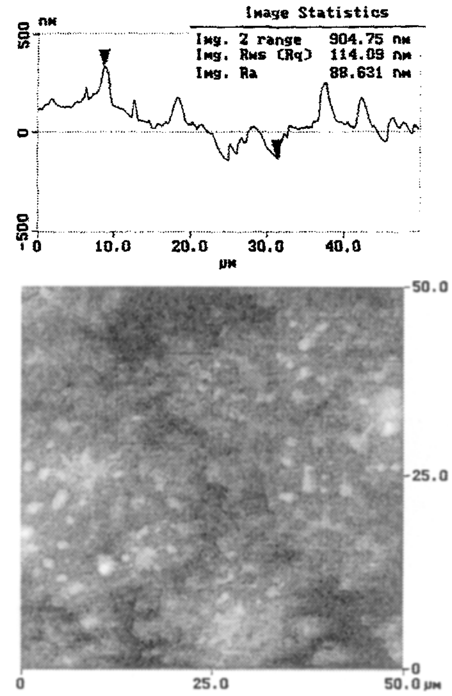

WC/Co 11% (Before) (Ra=88.63 nm)

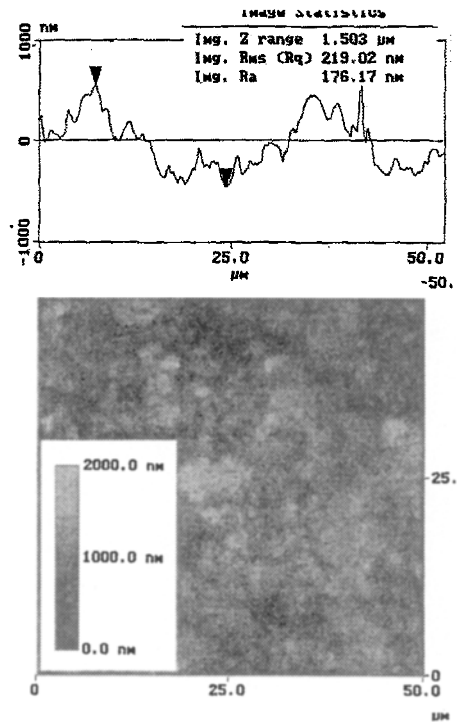

WC/Co 11% (After) (Ra=176.17 nm)

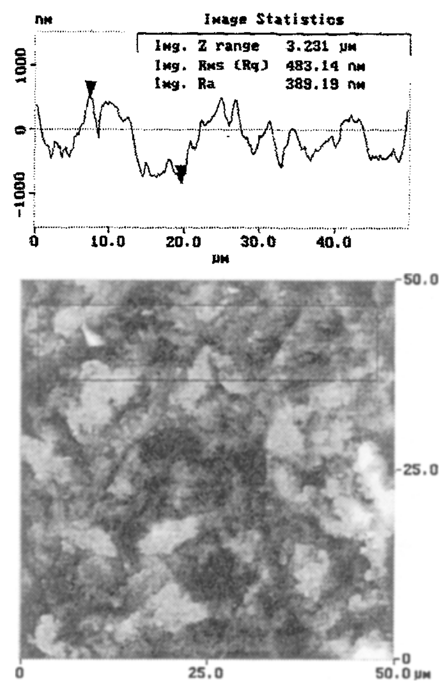

SAE 4340 (before) (Ra=389.19 nm)

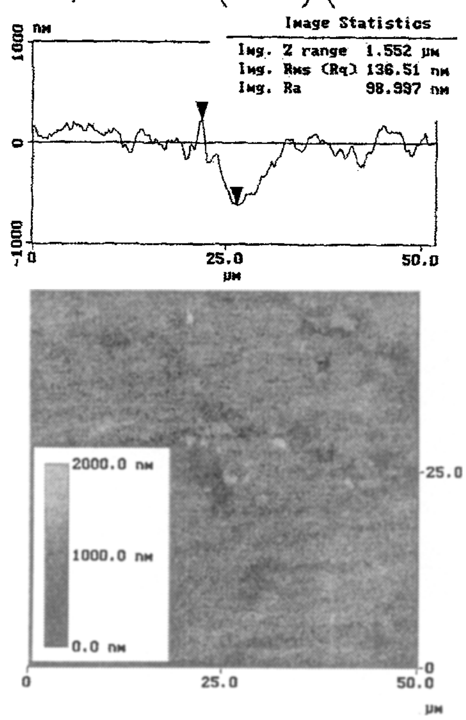

SAE 4340 (after) (Ra=98.997 nm)

Fig. 14—Atomic force microscope surface analysis of SAE 4340 steel sliding at 3.7 m/s against WC/Co 11 percent

Acknowledgments

The authors would like to thank Amos Gilat for the insight provided during discussions related to the design of the modified Kolsky bar. This research was supported by the National Science Foundation through Career Award No. CMS-9624364, by ONR-Young Investigator Award No. N00014-97-1-0550 and by the Army Research Office through MURI Grant No. DAAH04-96-1-0331. The second author was supported by the YPF S.A. Foundation through a J. A. Estenssoro Fellowship.

References

1. *Suh, N. P., Tribophysics, Prentice-Hall, Englewood Cliffs, NJ (1986).*
2. *Bhushan, B., Handbook of Micro/Nano Tribology, CRC Press, Boca Raton, FL (1995).*
3. *Ducker, W.A., Senden, T.J., and Pashley, R.M., "Direct Measurement of Colloidal Forces Using an Atomic Force Microscope," Nature,* **353**, *239–241 (1991).*
4. *Israelachvili, J.N., "Techniques for Direct Measurements of Forces Between Surfaces in Liquids at the Atomic Scale," Chemtracts Anal. Phys. Chem., 1–12 (1989).*
5. *Israelachvili, J.N., Intermolecular and Surface Forces, 2nd ed., Academic Press, London (1991).*
6. *Israelachvili, J.N., "Surface Forces and Microrheology of Molecularly Thin Liquid Films," Handbook of Micro/Nano Tribology, ed. B. Bhushan, CRC Press, Boca Raton, FL, 268–314 (1995).*
7. *Prakash, V. and Clifton, R., "Time Resolved Dynamic Friction Measurement in Pressure-shear," ASME,* **165**, *33–48 (1993).*
8. *Prakash, V., "Pressure-shear Plate Impact Experiment for Investigating Transient Friction,"* EXPERIMENTAL MECHANICS, **35**, *329–336 (1995).*
9. *Espinosa, H.D., Mello, M., and Xu, Y., "A Variable Sensitivity Displacement Interferometer with Application to Wave Propagation Experiments," J. Appl. Mech.,* **64**, *123–131 (1997).*
10. *Ogawa, K., "Impact Friction Test Method by Applying Stress Waves,"* EXPERIMENTAL MECHANICS, **37**, *398–402 (1997).*
11. *Anand, L., "A Constitutive Model for Interface Friction," Computational Mech.,* **12**, *197–213 (1993).*
12. *Anand, L. and Tong, W., "A Constitutive Model for Friction in Forming," Ann. CIRP,* **42**, *361–366 (1993).*
13. *Madakson, P.B., 1983, "The Frictional Behavior of Materials," Wear,* **87**, *191–206 (1983).*
14. *Feng, R. and Ramesh, K.T., "Rheology of Lubricants at High Shear Rates," Trans. ASME, J. Tribology,* **115**, *640–649 (1993).*
15. *Henry, S.D., ed., ASM Handbook, Friction, Lubrication and Wear Technology, American Society for Metals, Metals Park, OH (1992).*
16. *Martins, J.A.C., Oden, J.T., and Simões, F.M., "A Study of Static and Kinetic Friction," J. Eng. Sci.,* **28** *(1990).*
17. *Patanella, A.J., "A Novel Experimental Technique for Dynamic Friction Studies," Master's thesis, Purdue University (1998).*
18. *Kolsky, H., "An Investigation of Mechanical Properties of Materials at Very High Rates of Loading," Proc. Phys. Soc. London,* **62-B**, *676–700 (1949).*
19. *Kolsky, H., Stress Waves in Solids, Dover, New York (1963).*
20. *Duffy, J., Hawley, R.H., and Hartley, K.A., "The Torsional Kolsky (Split-Hopkinson) Bar," ASM Handbook,* **8**, *9th ed., American Society for Metals, Metals Park, OH (1985).*
21. *Gilat, A. and Pao, Y.H., "High-rate Decremental-strain-rate Test,"* EXPERIMENTAL MECHANICS, **28**, *322–325 (1988).*
22. *Kumar, P. and Clifton, R. J., "Dislocation Motion and Generation in LiF Single Crystals Subjected to Plate Impact," J. Appl. Phys.,* **50**, *4747 (1979).*
23. *Miyoshi, T., Takaya, Y., Takizawa, N., and Fukuzawa, R., "Development of Non-contact Profile Sensor for 3-D Free-form Surfaces (3rd Report)—Optical Ring Image 3-D Profile Sensor," J. Jap. Soc. Prec. Eng./Seimitsu Kogaku Kaishi,* **61**, *258–262 (1995).*
24. *Majumdar, A. and Bhushan, B., "Characterization and Modeling of Surface Roughness and Contact Mechanics," Handbook of Micro/Nano Tribology, ed. B. Bhushan, CRC Press, Boca Raton, FL, 268–314 (1995).*
25. *Espinosa, H.D., Patanella, A., and Fischer, M., "Dynamic Friction Measurements at Sliding Velocities Representative of High-speed Machining Processes," ASME J. Tribology (2000).*
26. *Brechet, Y. and Estrin, Y., "The Effect of Strain Rate Sensitivity on Dynamic Friction of Metals," Scripta Metallurgica et Materialia,* **30**, *1449–1454 (1994).*
27. *Ludema, K.C., Friction, Wear, Lubrication, CRC Press, Boca Raton, FL (1996).*
28. *Rabinowicz, E., "The Nature of the Static and Kinetic Coefficients of Friction," J. Appl. Phys.,* **22**, *1373–1379 (1951).*
29. *Blau, P.J., "Static and Kinetic Friction Coefficients for Selected Materials," ASM Handbook,* **18**, *American Society for Metals, Metals Park, OH, 70–75 (1992).*
30. *Larsen-Basse, J., "Introduction to Friction," ASM Handbook, Friction, Lubrication and Wear of Materials,* **18**, *ed. S.D. Henry, American Society for Metals, Metals Park, OH, 25–26 (1992).*
31. *Larsen-Basse, J., "Basic Theory of Solid Friction," ASM Handbook, Friction, Lubrication and Wear of Materials,* **18**, *ed. S.D. Henry, American Society for Metals, Metals Park, OH, 27–38 (1992).*
32. *Kendall, L.A., "Friction and Wear of Cutting Tools and Cutting Tools Materials," ASM Handbook, Friction, Lubrication and Wear,* **18**, *609–620 (1985).*